RESEARCH ARTICLE

Topographic and stochastic influences on pāhoehoe lava lobe emplacement

Christopher W. Hamilton · Lori S. Glaze ·
Mike R. James · Stephen M. Baloga

Abstract A detailed understanding of pāhoehoe emplacement is necessary for developing accurate models of flow field development, assessing hazards, and interpreting the significance of lava morphology on Earth and other planetary surfaces. Active pāhoehoe lobes on Kīlauea Volcano, Hawai'i, were examined on 21–26 February 2006 using oblique time series stereo-photogrammetry and differential global positioning system measurements. During this time, the local discharge rate for peripheral lava lobes was generally constant at 0.0061 ± 0.0019 m^3/s, but the areal coverage rate of the lobes exhibited a periodic increase every 4.13 ± 0.64 min. This periodicity is attributed to the time required for the pressure within the liquid lava core to exceed the cooling-induced strength of its margins. The pāhoehoe flow advanced through a series of down-slope and cross-slope breakouts, which began as ~0.2-m-thick units (i.e., toes) that coalesced and inflated to become approximately meter-thick lobes. The lobes were thickest above the lowest points of the initial topography and above shallow to reverse-facing slopes, defined relative to the local flow direction. The flow path was typically controlled by high-standing topography, with the zone directly adjacent to the final lobe margin having an average relief that was a few centimeters higher than the lava-inundated region. This suggests that toe-scale topography can, at least temporarily, exert strong controls on pāhoehoe flow paths by impeding the lateral spreading of the lobe. Observed cycles of enhanced areal spreading and inflated lobe morphology are also explored using a model that considers the statistical likelihood of sequential breakouts from active flow margins and the effects of topographic barriers.

Keywords Topographic influences · Stochastic processes · Pāhoehoe lava · Lobe emplacement

Introduction

Basalt is the most common rock type on the surface of terrestrial bodies throughout the solar system and—by total volume and areal coverage—pāhoehoe flows are the most abundant form of basaltic lava in subaerial and submarine environments on Earth (Self et al. 1996, 1997, 1998). Pāhoehoe flow fields are composed of flows, lobes, and toes, which represent a continuum of lava emplacement scales, with toes being the smallest elements. Pāhoehoe flows commonly advance as toes break out along lobe margins (Hon et al. 1994; Crown and Baloga 1999; Hoblitt et al. 2012). These new toes quickly cool and develop a rheological gradient that includes an inferred three-part structure composed of a brittle outer crust, underlying viscoelastic layer, and inner molten core (Hon et al. 1994). As toes develop sufficient strength to retain incoming lava, they can pressurize, coalesce, and inflate to form lobes that are interconnected with other portions of the flow through internal fluid pathways (Walker 1991, 2009). The evolution of these pathways can vary considerably (Kauahikaua et al. 1998), but the initial emplacement of pāhoehoe flow fronts can influence the subsequent development of the flow. Consequently, a detailed understanding of

C. W. Hamilton · L. S. Glaze
Planetary Geodynamics Laboratory, NASA Goddard Space Flight Center, Greenbelt, MD 20771, USA

C. W. Hamilton (✉)
Department of Astronomy, University of Maryland, College Park, MD, USA
e-mail: christopher.hamilton@nasa.gov

M. R. James
Lancaster Environment Centre, Lancaster University, Lancaster, UK

S. M. Baloga
Proxemy Research, Laytonsville, MD, USA

processes operating on the scale of toes and lobes can provide important information for modeling aspects of flow field development, assessing hazards, and interpreting the significance of lava flow morphology on Earth and other planetary bodies (Peitersen and Crown 2000; Byrnes and Crown 2001).

Hon et al. (1994) suggest that "microtopography" (i.e., tens of centimeters relief), herein termed "toe-scale topography," can strongly affect the emplacement of pāhoehoe lava flows that reach a final inflated thickness of several meters. Previous studies have attempted to determine the relationship between topography and pāhoehoe emplacement (Crown and Balgoa 1999; Peitersen and Crown 2000; Byrnes and Crown 2001), but these studies have been unable to quantify the effects of toe-scale topography at the flow front due to data resolution limitations. Here, oblique digital photogrammetry and differential global positioning system (DGPS) measurements are combined to quantify key physical parameters involved in pāhoehoe flow growth through the development of toes and lobes, which constitute the fundamental building blocks of all pāhoehoe flows (Walker 1991; Self et al. 1996, 1998; Thordarson and Self 1998). These field observations are also used to inform and constrain a new stochastic model that describes pāhoehoe lobe emplacement in terms of a balance between random and nonrandom processes.

Background

Pāhoehoe flow fields exhibit a multitude of branching events at several scales (Crown and Baloga 1999) and include self-similar morphologies (Bruno et al. 1994) that enable local observations to be used to understand larger aspects of flow fields and their emplacement. However, these patterns are complicated and irregular because of the influence of stochastic processes operating on multiple scales (Kilburn 1996). This makes it important to identify the scales over which recurring processes and structures combine to form the overall pattern of a pāhoehoe flow field. Understanding how eruption parameters, deterministic factors, and random influences affect the emplacement of pāhoehoe flows also makes it possible to develop improved probabilistic models to describe likely patterns of flow growth (Glaze and Baloga 2013). This study examines active pāhoehoe lava lobes on Kīlauea Volcano, Hawai'i, to characterize the effects of toe-scale topography on flow emplacement and identify key parameters needed to model statistical aspects of the process.

Pāhoehoe flows grow through a combination of areal spreading and inflation, with new toes breaking out along lobe margins and quickly cooling by radiation (Hon et al. 1994; Keszthelyi and Denlinger 1996; Harris et al. 2007a, Harris 2013). However, as time progresses and a thermally insulating skin develops on the surface of the new toes, the transfer of heat from the flow's interior becomes increasingly dominated by conduction (Keszthelyi and Denlinger 1996; Castruccio et al. 2013). The crust also helps to retain incoming lava, which slows the advance of the new toes as their internal pressure decreases relative to the increasing confining strength of the growing crust (Hon et al. 1994). Given a constant influx of lava, this leads to a reduction in the areal coverage rate of the toes and an increase in the rate of inflation. Inflation will then tend to dominate the emplacement process until the internal pressurization of the lobe reaches a threshold required to rupture the flow margins and initiate a new cycle of enhanced areal spreading (Hoblitt et al. 2012).

Within an active pāhoehoe flow, internal connections between numerous lobes can form extensive lava pathways (Kauahikaua et al. 1998). Preferred pathways within these lava networks will generally concentrate in existing topographic lows and may develop into a tube system as the surrounding flow cools and stagnates. This allows pāhoehoe flows to advance great distances by transporting lava to the flow front through thermally insulated pathways that can reduce cooling rates to only 0.5–1.0 °C/km (Harris and Rowland 2009). As lava is distributed from a master pathway into peripheral lobes and toes, the local discharge rates will progressively decrease with each branch in the system. Local discharge rates may therefore be constant over short periods of time (Hon et al. 1994), but are expected to evolve as the lobes at the former flow front are incorporated into the growing body of the lava transport system. In this study, lobes along the periphery of a low-discharge pāhoehoe flow are examined to explore flow front emplacement processes and inflation.

Study area

The Prince Kūhiō Kalaniana'ole (PKK) flow was erupted from Pu'u 'Ō'ō on Kīlauea Volcano, Hawai'i, from March 2004 to June 2007 (Fig. 1). Active margins along the flow were examined in the field between 21 and 26 February 2006. During this time, lava from Pu'u 'Ō'ō was primarily transferred though an established tube system that reached the ocean (Koeppen et al. 2013). However, during February 2006, the master tube system also fed a series of small surface flows located ~7 km south of Pu'u 'Ō'ō. Harris et al. (2007a) referred to this portion of the PKK flow as the "Hook flow." Field observations and thermal imagery were used to establish that the Hook flow exhibited breakouts of S-type pāhoehoe (Wilmoth and Walker 1993) from three small flows on 21 February. However, by 23 February, the activity had dwindled to the distal margin of just one flow. Waning activity was also evidenced by a decrease in maximum core temperature from 1,141 °C on 21 February to 1,131 °C on 23 February and a decrease in areal coverage rate from ~0.22 m^2/s on 22 February to ~0.03 m^2/s on 23 February (Harris et al. 2007a). Additionally, there was a corresponding decrease in discharge

Fig. 1 Lava flow map showing the study area location (19.336430° N, 155.055235° W) within the Prince Kūhiō Kalaniana'ole flow (shown in *yellow*) on Kīlauea Volcano, Hawai'i. Pāhoehoe lava lobes at this locality were fed lava from Pu'u 'Ō'ō. Field measurements were acquired on 21–26 February 2006 for two lobes (A and B) located along the same lava pathway system. Lobe B was located directly down-slope of Lobe A, with a separation distance of ~10 m. The *dashed lines* approximately bound the edifices of Pu'u 'Ō'ō and Kupaianaha. Lava flow data provided by Tim Orr, United States Geologic Survey
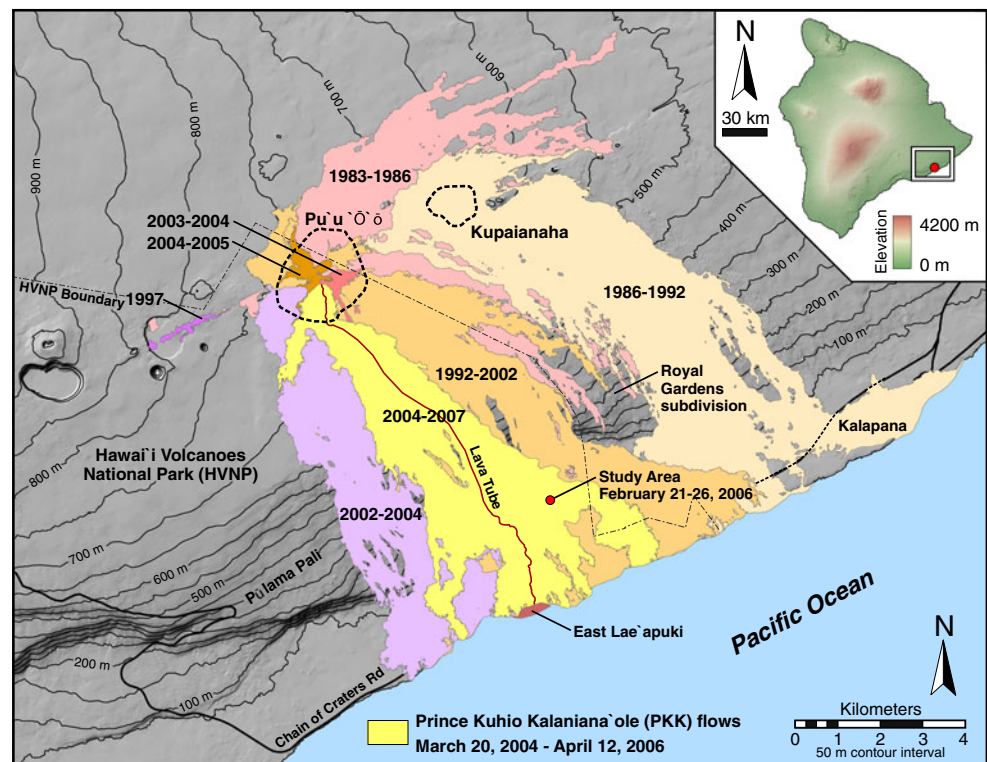
rate feeding small surface flows, from ~0.14 m³/s on 22 February to ~0.03 m³/s on 23 February (Harris et al. 2007a). These surface flows stagnated on 24 February. Measurements reported in this study were made contemporaneously with the observations of Harris et al. (2007a), who used thermal image chronometry to establish broad relations among cooling, discharge rate, and areal coverage rates for the whole flow.

To place the local lava discharge rates into a broader context, the Pu'u 'Ō'ō-Kupaianaha eruption began erupting in Kīlauea Volcano's East Rift Zone (ERZ) on 3 January 1983, and between 1983 and 2002, its time-averaged discharge rate (Harris et al. 2007b) was ~3.81 m³/s dense-rock-equivalent lava (Heliker and Mattox 2003). However, the Pu'u 'Ō'ō-Kupaianaha eruption has undergone numerous changes throughout its history (Heliker and Mattox 2003), and in 2003–2007, the magma supply rate to the ERZ increased significantly during a mantle-derived surge to Kīlauea Volcano (Poland et al. 2012). During this time, the magma supply to Kīlauea Volcano increased by a factor of 2 (Poland et al. 2012). By 2005, the supply rate to the ERZ increased to ~5.11 m³/s (Poland et al. 2012), and so at the time of the field campaign in February 2006, effusion rates from Pu'u 'Ō'ō were probably higher than the long-term average. Tilt meter records from the Hawaiian Volcano Observatory's Pu'u 'Ō'ō cone station also show that there was an oscillatory pattern of inflation and deflation between 21 and 26 February 2006 (Orr 2011). This pattern began with an inflation event on 21 February, which was followed by gradual deflation over the

next 5 days through a series of smaller tilt cycles (Tim Orr, personal communication, 2013). Orr (2011) showed that these tilt cycles were associated with fluctuations in lava discharge through the tube system and may have contributed to the observed breakouts from the master tube. Discharge rates associated with the small surface flows examined within this study were therefore much lower than for the concurrently active PKK tube and for the Pu'u 'Ō'ō-Kupaianaha eruption as a whole.

Methods of digital terrain modeling

To quantify the aspects of the pāhoehoe emplacement processes, two complementary methods were employed. First, time series oblique stereo-imaging and photogrammetry (Robson and James 2007) were used to determine the changing geometric properties of an active lava lobe, herein referred to as Lobe A. Second, DGPS measurements of topography before and after the emplacement of a second pāhoehoe lobe (Lobe B) were used to assess the relationship between initial topography and final lobe morphology. Lobes A and B were located along the same lava pathway system, with Lobe B located ~10 m directly down-flow of Lobe A (Fig. 1).

Time series stereo-image pairs of Lobe A were acquired on 23 February using two synchronized tripod-mounted digital single-lens reflex cameras (6 megapixel Canon EOS 300D), which collected image pairs every minute over a duration of

35 min (Robson and James 2007). The cameras were mounted approximately 1 m apart and had pre-calibrated, fixed-focus 28-mm lenses. Photogrammetric control was provided using spherical targets (25 mm in diameter) with positions determined by the DGPS measurements. The analysis was carried out using Vision Measurement System (Robson and Shortis, http://www.geomsoft.com) with image matching by the GOTCHA dense matching algorithm (Gruen 1985; Day and Muller 1989; Otto and Chau 1989). A typical stereopair provided topographic point cloud data with positional precisions of 25, 65, and 20 mm in easting (x), northing (y), and elevation (z), respectively. To quantify surface changes, these point cloud data were gridded in Surfer using a kriging algorithm over a 0.1-m/pixel x–y grid. The data were then imported into ArcGIS.

For Lobe B, x, y, and z coordinates for topographic surfaces were acquired before (23 February) and after lava emplacement. Post-emplacement surveys were performed on 24–26 February. However, no changes were observed after 24 February and so data from these three surveys were combined together. Data were collected at a sampling rate of 0.5 s using two Ashtech Z-Xtreme DGPS receivers—one operating in kinematic mode and the other as a static base station. These data were post-processed using Ashtech Solutions 2.60 with differential, L1/L2 (1,575.42/1,227.60 MHz) frequency correction for ionospheric delay error, and International Global Navigation Satellite System Service Standard Product 3 precise orbit file corrections. Resulting data points were filtered to remove measurements with more than 0.05 m residual accuracy error. On volcanic terrains, Hamilton et al. (2010) estimate the vertical precision of single traverse kinematic DGPS surveys to be ±0.08 m, and double traverses being ±0.06 m, with horizontal precision being better than the vertical measurements. Most gridded cells in this dataset contain multiple DGPS observations and should have a vertical precision of ±0.06 m. The resulting datasets for the initial and final topography include 14,618 and 20,585 records, respectively. To avoid spatial aliasing and to eliminate redundant data, the BLOCKMODE function in Generic Mapping Tools (GMT; Wessel and Smith 1991) was used to average z within each pixel. Filtered x, y, and z, data were then interpolated using NEARNEIGHBOR in GMT to form a 0.1-m/pixel x–y grid.

Time series observations of pāhoehoe lobe emplacement

Stereogrammetric point clouds and interpolated digital terrain models (DTMs) were used to identify and digitize the active margins of Lobe A at 1-min intervals (Fig. 2). These areal spreading maps show that the lava lobe grew by a series of breakouts that broadly fit into two categories: narrow (0.2–0.6-m-wide) toes that grew preferentially down-slope and broad (1.4–3.5-m-wide) breakouts that formed along the sides of the lobe, nearly perpendicular to the down-flow axis (Figs. 3 and 4). Initial toe thicknesses were typically ~0.2 m and, during the 35-min period of observation, they inflated to a maximum thickness of ~1.1 m, with most toes inflating to half their final observed thickness within 10 min. Within the first minute of emplacement, toes generally extended ~0.2 m, with a range of 0.05 to 0.55 m. After 28 min, the active flow margin began to exit the field of view of the stereo-cameras, and toe lengths could not be accurately constrained.

The mean local discharge rate measured at Lobe A over the first 19 min was 0.0061 ± 0.0019 m^3/s ($N=19$, Fig. 5a). Note that all uncertainties in this study are reported at 1 standard deviation, σ, unless otherwise noted. Standard deviation describes how much variation there is from the mean, whereas standard error on the mean, σ_μ, provides a measure of how well the mean itself is known based on the number of data points, N, used in the calculation. We therefore provide N as well as σ to enable the calculation of $\sigma_\mu = \sigma/\sqrt{N}$. After 35 min, the lobe covered a new area of 11.7 m^2 and achieved a cumulative volume of 10.4 m^3.

This local discharge rate was remarkably constant during the observation period, except for the interval between 19 and 24 min, when it decreased by nearly a factor of 4. During this interval, the lobe experienced little inflation and had generally lower than average areal spreading rates (Fig. 5a). However, this may have been due to breakouts occurring outside the field of view. At 24 min, the local discharge rate of 0.0061 m^3/s resumed, but after 28 min, the measured rate of volume change gradually decreased as the active flow front began to exit the field of view of the stereo-cameras. The mean areal coverage rate was 0.0055 ± 0.0038 m^2/s ($N=35$), but exhibited a cyclicity with peaks ~3 times greater than the mean (Fig. 5b), with a period of 4.13 ± 0.64 min ($N=8$). During each cycle of areal enhanced growth (measured from trough to trough in areal coverage rates shown in Fig. 5b), the lobe covers a new area of 1.59 ± 0.28 m^2 ($N=7$).

In this study, excess lobe volume is defined as the volume change in the field of view per minute minus the change in area during that minute, multiplied by the typical initial thickness of the new breakouts. Excess lobe volume is significant because it accounts for the change in lobe volume that is not directly attributable to its areal expansion. The typical thickness of new breakouts from Lobe A was ~0.2 m, but may vary for other flows—generally scaling with local discharge rate (Self et al. 1998). Excess volume changes for Lobe A appear to be weakly anti-correlated with its areal spreading rate. However, to quantify the degree of anti-correlation, the Pearson cross-correlation coefficient (Sheskin 2011) was calculated between areal growth and excess volume. The correlation analysis was restricted to the first 19 min of observation when the volume flow rate feeding the lobe was relatively constant. The areal growth rate during this 19-min period exhibits a

Fig. 2 Orthorectified view of photogrammetric point cloud at time $t=35$ min for Lobe A, with overlaid lava flow boundaries shown at 1-min intervals and the locations of the down-slope $\left(\overline{AA'}\right)$ and cross-slope $\left(\overline{BB'}\right)$ profiles shown in Fig. 4
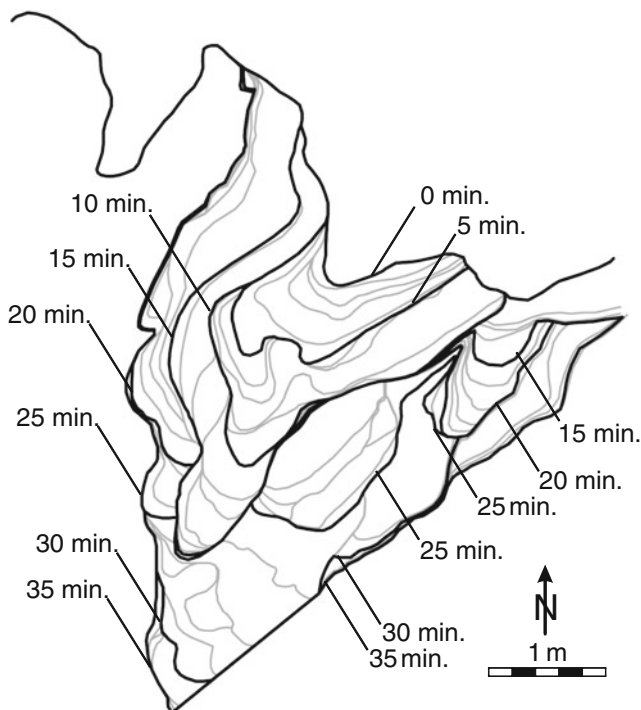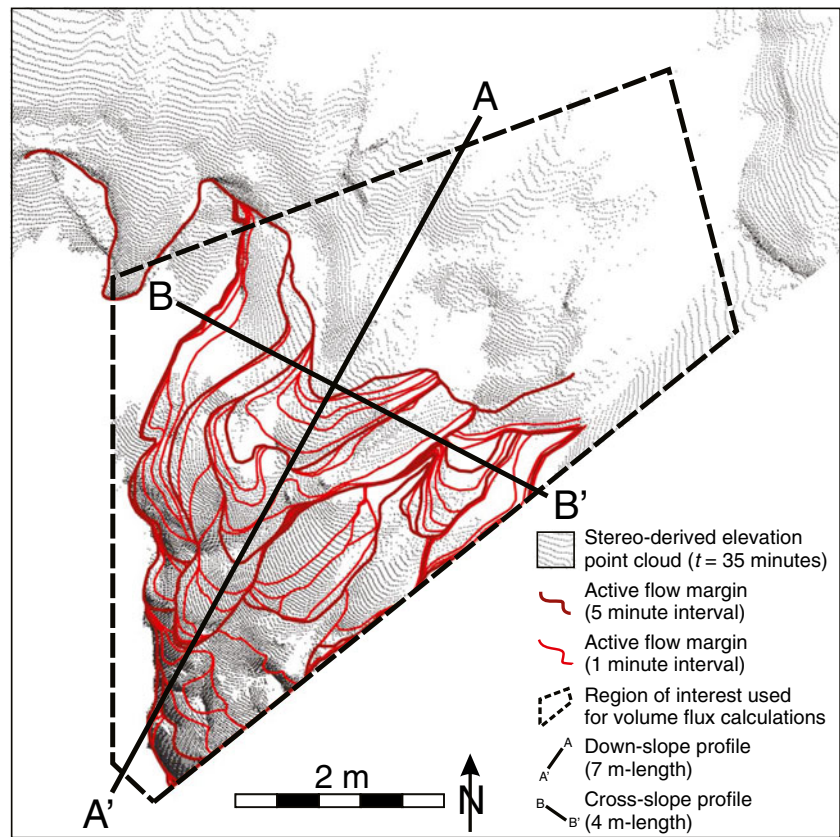

Fig. 3 Time series evolution of Lobe A. Dark lines show the extent of the flow at 5-min intervals with gray lines showing the flow margins at 1-min intervals. The flow begins to move outside the field of view at 28 min

slight overall increase over time (slope=0.013 m²/min² and intercept=0.206 m²/min), and therefore, the trend was removed prior to analysis. After trend removal, the Pearson cross-correlation coefficient, at lag=0 (i.e., the measure of direct anti-correlation), is −0.22. The negative sign of this statistic indicates anti-correlation; however, the magnitude is well within the 90 % confidence interval (±0.34) indicating that the anti-correlation is very weak and not statistically significant at this level. This suggests that there may be a trade-off between areal spreading and inflation given an approximately constant lava supply, but that the relationship may be complicated by other factors. See "Model simulations of areal growth" section for further discussion.

Lava thickness, inflation, and the effects of topographic relief on pāhoehoe lobe emplacement

Topographic maps of the terrain before and after the emplacement of Lobe B are shown in Fig. 6. Lava covered 111.83 m² within the DGPS survey region, with a total lobe volume of 59.45 m³. Forward looking infrared radiometer (FLIR) measurements of the flow at 06:00 on 24 February 2006 revealed no anomalously hot pixels within the study region, which indicates that the flow terminated at least 5 h before (Harris

Fig. 4 a Down-slope $\left(\overline{AA'}\right)$
and **b** cross-slope $\left(\overline{BB'}\right)$ profiles
for Lobe A showing the changing
topography of the lava lobe
shown in Figs. 1 and 2
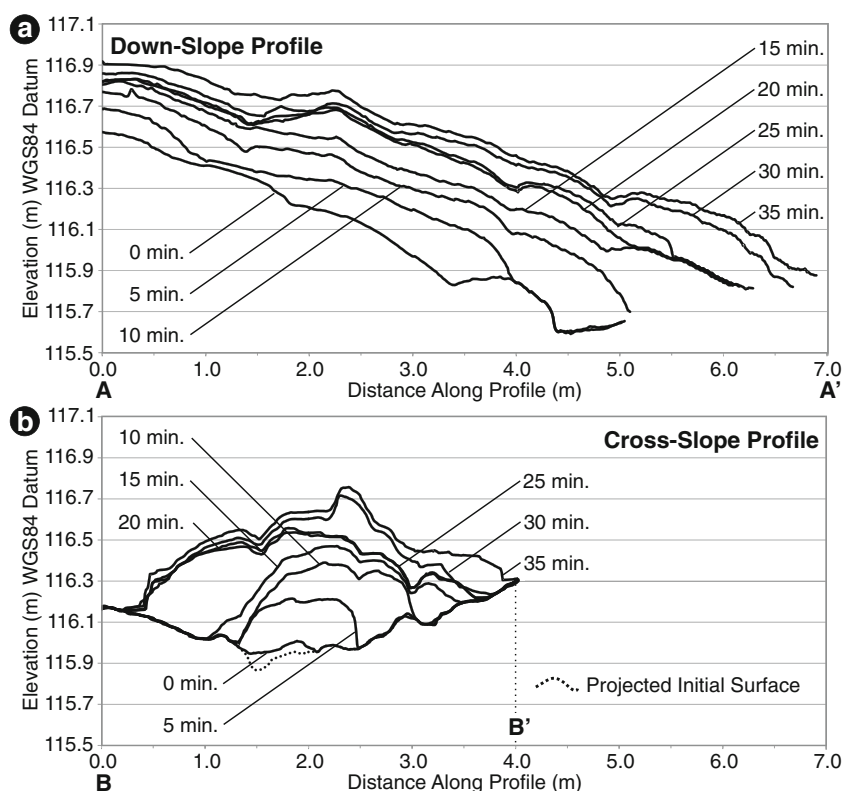
et al. 2007a). Based on the time of the last field observations on 23 February, this constrains the emplacement duration to <8 h. If the mean areal coverage and discharge rates were similar for Lobes A and B, then the emplacement duration of Lobe B was likely between 2.6 and 5.2 h.

Using the before and after DTMs (Fig. 6a, b), topographic profiles have been extracted down-slope (Fig. 7a) and cross-slope (Fig. 7b). The lava entered the study region from the north, and the lobe grew to a length of ~18 m and a maximum width of 9.1 m. However, the distal part of the flow focused into a 4.3-m-wide topographic constriction before being bi-furcated by a 1.0-m-high topographic obstacle into two small-er lobes that were 2.4- and 4.0-m-wide. The profiles show that inflation of the lava tended to topographically invert the landscape, with the thickest portions of the lobe developing above topographic depressions and shallow to reverse-facing slopes, defined relative to the local flow direction. Thus, apparent barriers to the spreading of the flow are typically much smaller than the maximum height of the lobe, and the thicker portions of the lobe appear confined by the thinner peripheral parts of the flow.

The thickness of Lobe B above the existing surface (Fig. 6c) was calculated by taking the simple difference between the final and initial topography. This yields a mean lobe thickness of 0.57±0.24 m, with a maximum of 1.21 m. However, this simple topographic difference overestimates inflation because lobes are initially emplaced as toes with an initial thickness. Additionally, lava had to fill small closed

depressions before thickening above the surrounding topography.

To account for the infilling of small topographic depres-sions, a new initial surface was created by smoothing the initial topography in a process that is analogous to tightly stretching a rubber sheet through the data. The smoothed surface was created using the GMT function SURFACE, which interpolates a grid using continuous curvature splines in tension (Smith and Wessel 1990). Specifically, the SUR-FACE applies the Laplace transform (L) to the initial topog-raphy (z):

$$(1-T)L \times (L(z)) + T \times L(z) = 0. \qquad (1)$$

Varying the tension factor T between 1 (i.e., the harmonic surface solution) and 0 (i.e., the minimum curvature solution) enables this data interpolation method to smooth the initial surface to different degrees. For instance, a grid produced with high tension ($T \rightarrow 1$) will suppress local maxima and minima by fitting an increasingly taut surface between the data con-straints, whereas applying a looser tension factor ($T \rightarrow 0$) will produce a smooth polynomial function analogous to a flexed elastic plate that is anchored by the data (Smith and Wessel 1990).

To constrain the inflated thickness of Lobe B, a smoothed local datum was fit to the initial topography using a T value of 1. This removes high-frequency oscillations in the topog-raphy, while preserving the overall shape of the terrain.
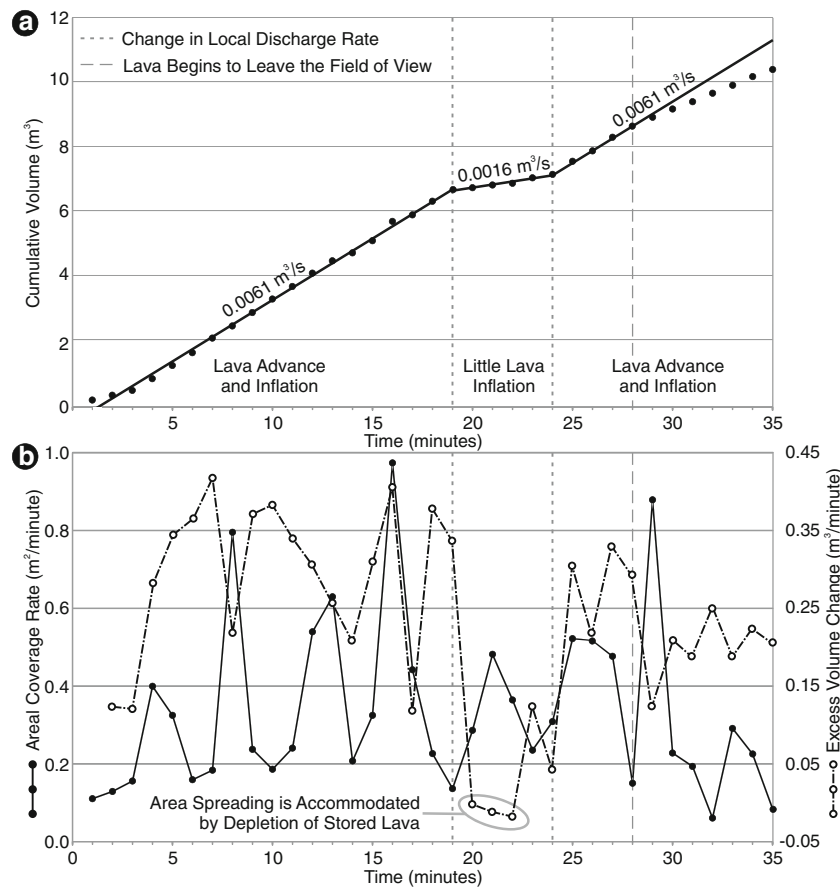
Fig. 5 **a** Cumulative volume in the region of interest identified in Fig. 2 for Lobe A. The mean local discharge rate (0.0061±0.0019 m³/s, calculated for the first 19 min) is generally constant during the observation period, except for the interval between 19 and 24 min where the mean local discharge rate decreases by nearly a factor of 4 and the lobe experiences little inflation and generally lower than average areal spreading rates. At 28 min, the rate of volume change gradually decreases as the active flow front begins to exit the field of view of the stereo-cameras. **b** Areal coverage rate (mean 0.33±0.23 m²/min, *filled black circles with solid black line*) and mean excess volume change (0.23±0.12 m³/min, *open circles with broken line*), where excess volume change is defined in the text. Excess volume change less than 0, between 20 and 23 min, implies that areal growth was accommodated by depletion of stored lava during this time interval. The areal coverage rate shows a periodicity with peaks at intervals of 4.13±0.64 min. All uncertainties are reported at 1σ

Subtracting this surface from the final topography isolates the thickness of lava above the local datum and provides a better proxy for inflation than the simple difference map because it reduces the thickness contributions due to small basin infilling. Using this method, the mean thickness due to inflation was 0.34 ±0.21 m (N=9614), with a maximum of 1.00 m (Fig. 6d).

To isolate local relief within the initial topography, a second interpolated surface was created using Eq. (1) with T=0.25. A loose tension factor of T=0.25 is recommended for low-tension interpolations to suppress extraneous oscillations (i.e., minima and maxima) that can otherwise be generated when using the end-member minimum curvature solution (i.e., T=0; Wessel and Smith, http://gmt.soest.hawaii.edu/). The new surface preserves more variations in the initial topography than the harmonic surface solution (T=1) and was subtracted from the original initial topography to isolate high-frequency changes in elevation (i.e., relief) above and below a new local datum centered on 0 m.

In the lava-inundated region, the distribution of initial relief is unimodal with a mean of −0.02±0.07 m (N=9,614 pixels; Fig. 8). For comparison, a 1-pixel buffer region was also defined around the outer extent of the lobe and, in this buffer region, the frequency distribution of relief had a mean of 0.00±0.07 m (N= 499 pixels). However, relative to the lava-inundated region, there are more pixels with a relief of 0.03 to 0.09 m and fewer pixels with a relief of −0.09 to −0.03 m (Fig. 8). This means that there are systematically more high relief pixels bounding the pāhoehoe lava lobe than in the region that was inundated. Consequently, positive relief on the order of only a few centimeters may exert an important influence on bounding the extent of low effusion-rate pāhoehoe flows.

Toe-scale topography (i.e., on the order of centimeters in this case) appears to influence the areal spreading of pāhoehoe lobes by blocking peripheral toes, which may then stagnate and help to confine the interior portions of the flow. If the interior of the flow continues to be supplied by lava, it may

Fig. 6 **a** Initial and **b** post-lava lobe emplacement DTMs generated from DGPS measurements for Lobe B, with *cool colors* showing low elevation and *warm colors* showing relatively higher elevation. **c** Simple difference between the final and initial topography. **d** Difference between the final topography and a Laplacian harmonic surface solution, which removes the effects of closed basin filling. Profiles $\left(\overline{CC'}\right)$ and $\left(\overline{DD'}\right)$ are shown in panels a and b of Fig. 7, respectively. Elevations in (**a**) and (**b**) are reported relative to the WGS84 datum, and lava thicknesses in (**c**) and (**d**) are shown to the same scale
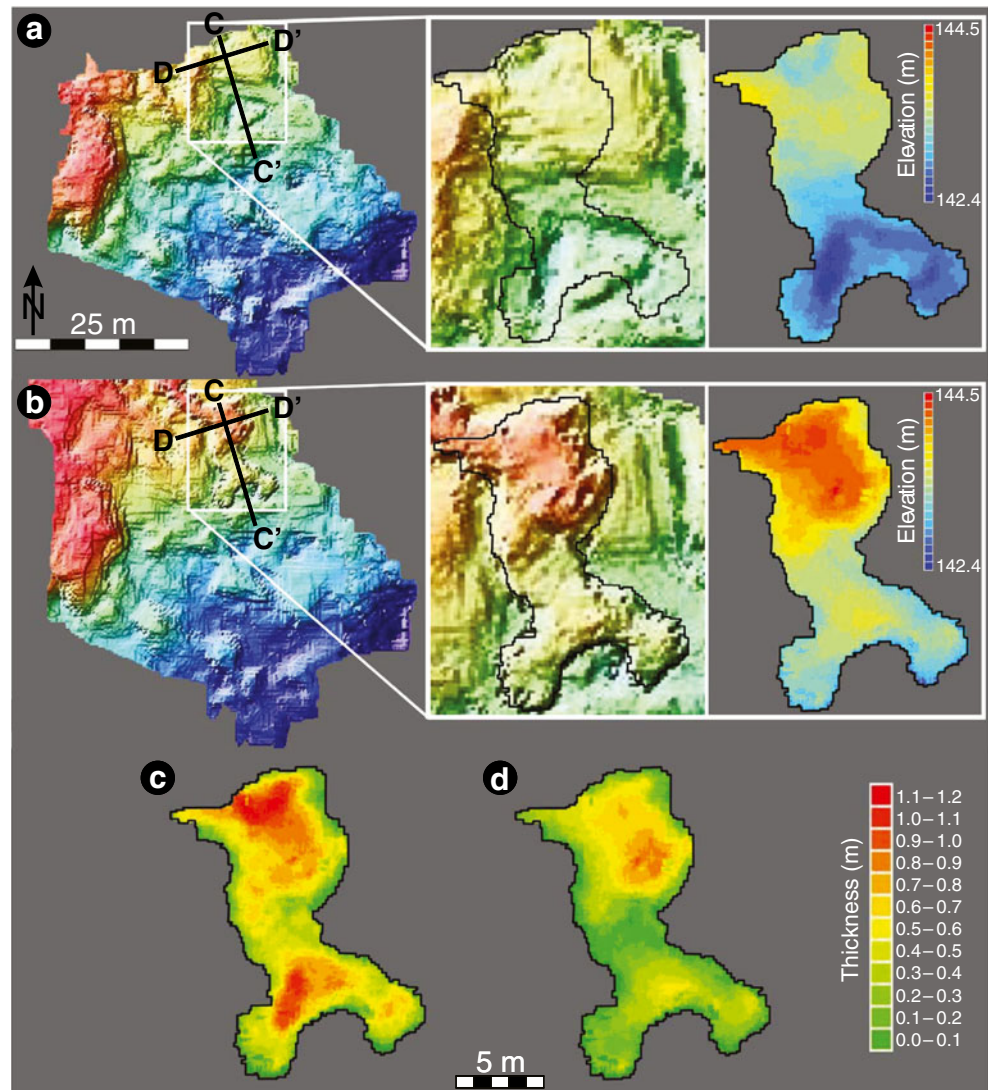
then inflate above the height of surrounding barriers, thereby topographically inverting the landscape. Barriers to flow may therefore be much less than the final inflated thickness of a lobe. Based on observations of Lobe B, relief that is at least 15 % of a toe's initial thickness may be significant in terms of affecting the path of low-discharge pāhoehoe lava lobes, but given sample size-dependent restrictions on the optimum bin size for the data (Sturges 1926; Doane 1976), influences of even smaller variations in topography cannot be precluded. Obstacle heights affecting the path of higher local discharge rate flows may also scale with initial toe height.

Stochastic modeling of pāhoehoe lobe emplacement

Overview of the model

Random effects strongly influence the processes of pāhoehoe flow growth and pose a fundamental difficulty in

developing models for their emplacement (Hon et al. 1994; Thordarson and Self 1998; Keszthelyi et al. 1999; Crown and Baloga 1999). Glaze and Baloga (2013) have recently developed a new simulation approach for modeling pāhoehoe emplacement that builds on the ideas presented in Baloga and Glaze (2003). This model is based on (1) conservation of lava volume and (2) prescribed stochastic rules for lava movements within a pāhoehoe lobe. This approach differs significantly from other models that treat lava emplacement as a gravity-driven viscous fluid flow on an inclined plane (e.g., Danes 1972; Hulme 1974; Baloga and Pieri 1986; Baloga 1987; Crisp and Baloga 1990; Harris and Rowland 2001; Rowland et al. 2004; Baloga and Glaze 2008). The Glaze and Baloga (2013) model simulates the three-dimensional shape for pāhoehoe lobes as they evolve in time, subject to a wide variety of ambient and internal conditions and processes. Here, the new model is used to explore the effects of inflation on pāhoehoe lobes analogous to Lobes A and B.

Fig. 7 **a** Down-slope and **b** cross-slope profiles showing the initial and final topography for Lobe B (see $\overline{CC'}$ and $\overline{DD'}$ in Fig. 6). The flow has topographically inverted the landscape, with inflation being greatest above paleo-topographic lows and anti-facing slopes, and least above forward-facing slopes. Note the pre-eruption topography and thin confining flow margins that may help to confine the thicker interior portions of the lobe
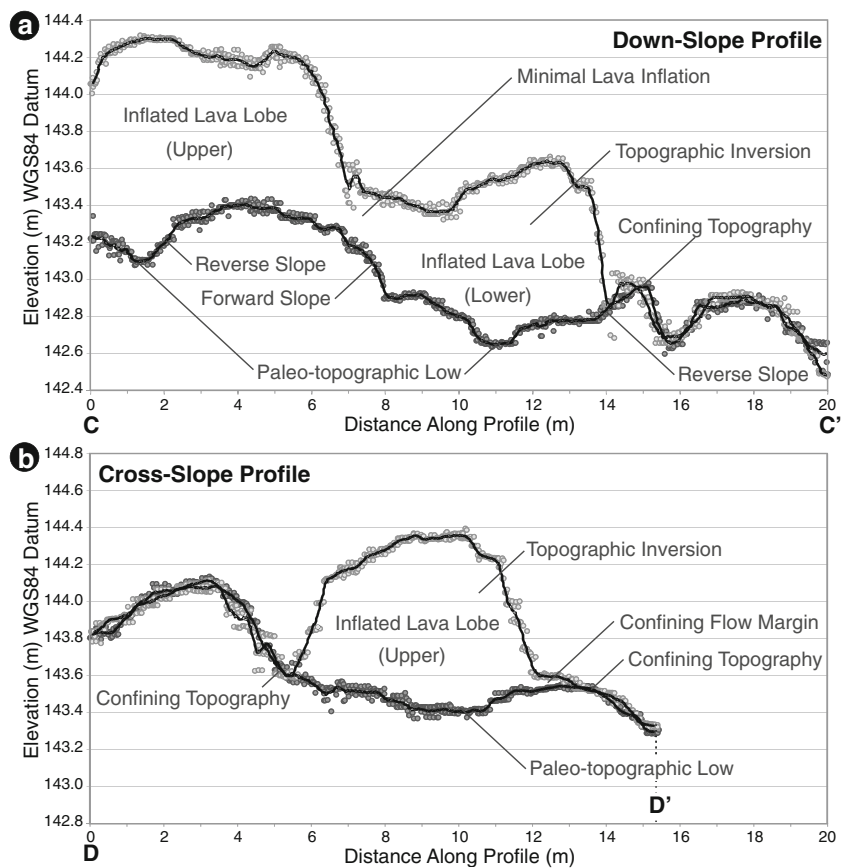
The fundamental building block of the Glaze and Baloga (2013) model is the lava "parcel." A parcel of lava is defined here as a volumetric unit sampled from a probability distribution of lava volumes that typically construct a pāhoehoe lobe. Thus, the smallest toe observed on the surface or along the margins of a pāhoehoe lobe may represent a lava parcel volume from the small end of the distribution. However, larger toes may either represent a larger parcel volume or may be comprised of multiple parcels.

A parcel is observable as a "toe" when it is permanently affixed at the surface or margin of a lobe. In the Glaze and Baloga (2013) model, lava parcels originate from a source
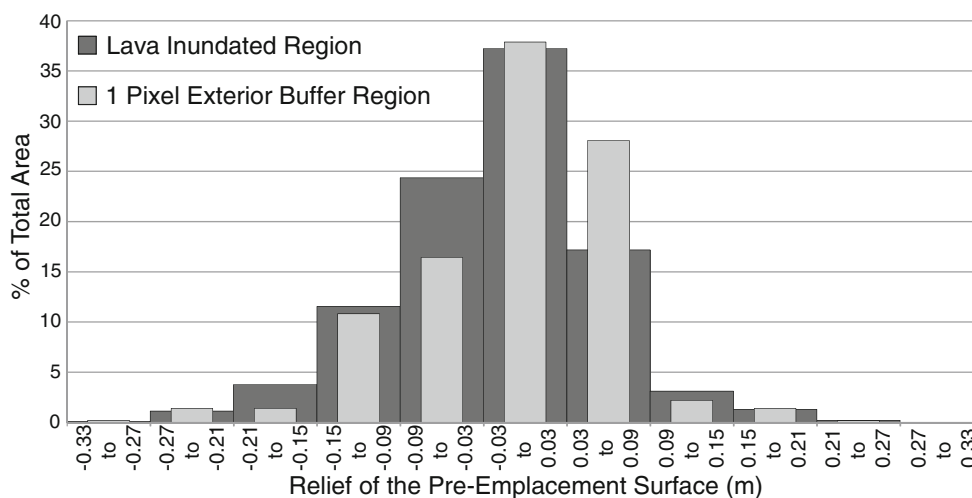
Fig. 8 Frequency distribution of relief on initial surface within the lava-inundated region (*dark gray*) and within a 1-pixel buffer region around Lobe B (*light gray*). The mean relief within both regions is close to 0 (i.e., 0.02±0.07 m in the inundated region and 0.00±0.07 m in the buffer region), but the buffer region exhibits more +0.03 to +0.09 m relief surfaces and −0.09 to −0.03 m relief surface, which implies that positive relief on the order of only a few centimeters may act to confine the areal spreading of the flow. All uncertainties are reported at 1σ
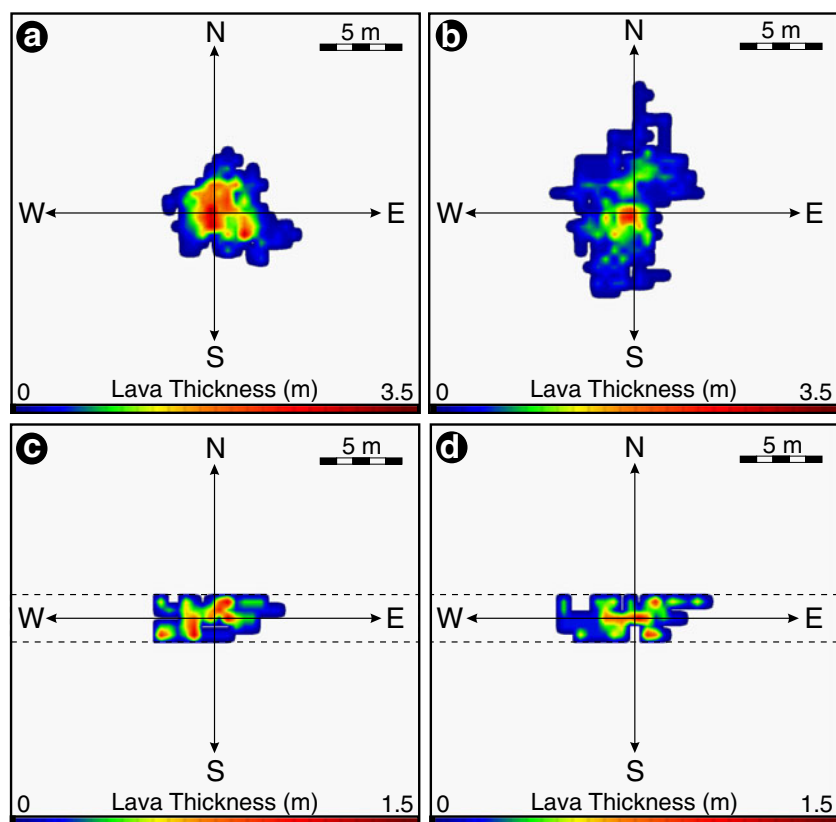
Fig. 9 **a** Simulation of 500 randomly emplacement lava parcels (without sequential breakouts from lobe margins). The maximum flow thickness is 3.2 m. **b** Simulation of 500 lava parcels using the same probability distribution for correlated toe growth used to model Lobe A (i.e., $P(0)=P(1)=0.25$ and $P(2)=0.5$). The maximum flow thickness is 2.6 m. Note that including correlated breakouts in (**b**) increases the perimeter/area ratio relative to the random example shown in (**a**). **c**, **d** Plane view examples of two simulations of Lobe A using 117 lava parcels, boundaries (*dash lines*) at ±3 cells on the north–south axis, and a probability distribution of $P(0)=P(1)=0.25$ and $P(2)=0.5$ for adding 0, 1, and 2 extra parcels in the same direction when a parcel breaks out from the flow margin. The maximum height of the flows shown in (**c**) and (**d**) are 1.2 m. For visualization purposes, the REBIN function in Interactive Data Language (IDL) was used to magnify the cells by a factor of 10 and perform a default bilinear interpolation. This process smoothes the model output and provides the exterior toes with a rounded appearance. This process does not alter the raw model output shown in Fig. 10 or 11b

region and are transported through fluid internal pathways. For the purposes of discussion here, the model assumes a constant parcel size for all parcels. Crown and Baloga (1999) measured dimensions of hundreds of toes, and their mean thickness is very well constrained at ~0.20 cm (0.19±0.08 m, $N=448$). Based on the geometric mean toe sizes measured by Crown and Baloga (1999), the parcel volume is assumed to be 0.09 m^3 (Glaze and Baloga 2013). Assuming a square x–y grid and a typical parcel thickness of 0.2 m—comparable to the observed initial thickness of toes in our study area—the corresponding cell spacing is 0.67 m, with a parcel area of 0.45 m^2.

The Glaze and Baloga (2013) random simulation model begins with an initial source region (a single point, linear source, etc.), a constant supply of lava (i.e., one parcel per time step), and probabilistic rules governing where each parcel will be transferred and allocated. For example, in the most basic scenario of complete randomness, two random choices are made for each breakout. First, a parcel is randomly selected to be the source for the next parcel transfer. Second, a random

selection is made to determine the orientation of the new parcel transfer relative to its source (i.e., north, south, east, or west). In the purely random case, every face of every parcel has an equal probability of being the source for the next parcel transfer. As various factors that influence emplacement are examined (e.g., barriers, slope, etc.), different probabilistic rules are applied that determine where and when each parcel will be transferred.

Model simulations of areal growth

Figure 9a shows a typical example of a completely random simulation involving 500 parcels. In this simulation, each transfer location and direction are chosen at random. Figure 10a (solid line) shows the corresponding cumulative area as a function of time step. However, Glaze and Baloga (2013) showed that topographic profiles of pāhoehoe lobes are more consistent with simulations that include sequential breakouts at the margin. In this case, the momentum of new parcels breaking out from a lobe margin results in an increased
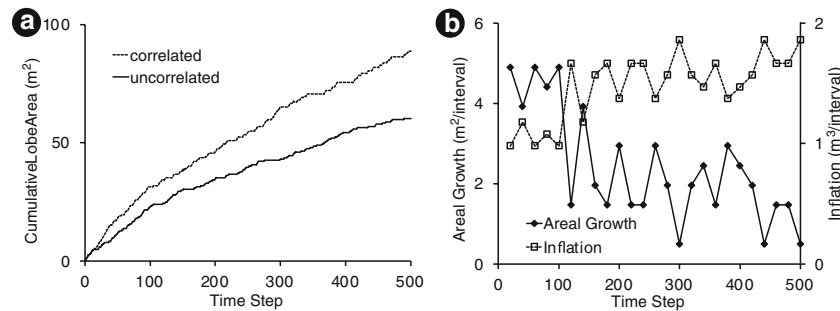
Fig. 10 a Cumulative lobe area versus time for two stochastic simulation realizations of pāhoehoe lobe emplacement. The uncorrelated realization (*lower solid line*) was generated by considering purely random selection of both the location and direction of each parcel transfer. The correlated scenario (*upper dashed line*) modifies this model by introducing an increased probability of sequential parcel emplacement when new parcels break out at the periphery of the flow. In this case, the probabilities of adding 0, 1, and 2, correlated parcels are $P(0)=0.25$, $P(1)=0.25$, and $P(2)=0.5$, respectively. **b** Periodicities and anti-correlation in areal spreading and excess volume change for a typical purely random simulation and an interval of 20 time steps

probability that the next parcel will be transferred from the most recent parcel in the same direction. Figure 9b shows the influence of allowing sequential breakouts at the lobe margin on lobe morphology. Specifically, every time a new parcel is transferred to the margin (increasing the lobe area), probabilistic rules are used to determine whether 0, 1, or 2 extra parcels will be added at that location. For the simulation shown in Fig. 9b, the probability of 0 additional parcels is $P(0)=0.25$, of 1 additional parcel being added is $P(1)=0.25$, and of 2 additional parcels is $P(2)=0.5$. As expected, the cumulative area of the simulation that includes sequential breakouts at the margin rapidly diverges from the purely random simulation (Fig. 10a), exhibiting a steeper gradient and overall greater cumulative area. Although a general trend in the areal growth (cubic meter per time step) is evident in both simulations (Fig. 10a), the curves are irregular with periods where the area increases rapidly and periods where the area does not change at all. Also as expected, the rate of overall areal growth tapers off over time as the number of available lava transfer locations along the margins decreases relative to the total area of the lobe.

The Glaze and Baloga (2013) simulation approach explicitly requires that lava parcels will either expand the area of the flow or contribute to inflation if they are allocated to the flow interior. This naturally results in a trade-off between areal growth and interior lobe inflation similar to the pattern observed during the emplacement of Lobe A. The natural periodicity of the areal growth rate in the simulated lobes is illustrated by the solid line in Fig. 10b. Also shown in Fig. 10b is the excess volume, which was defined in "Time series observations of pāhoehoe lobe emplacement" section as the volume above what is directly associated with the change in lobe area. This distinction is required because all breakouts will be emplaced with some initial thickness. For the simulated data, the definition of excess volume results in a periodic behavior that exactly mirrors the areal growth (i.e., perfect anti-correlation). This suggests that the weak anti-correlation

shown in Fig. 5b may be relevant, but that other processes are present in the field that have not yet been accounted for by the model. Also in the field example, there was a period of anomalously low average lava flux between 20 and 23 min, which coincided with a period of negative excess volume change. This indicates that areal spreading can also be accommodated by the depletion of lava stored within the parent lobe, rather than always being related to a simple balance between pressurization and confining strength under conditions of constant lava supply. Future studies would therefore benefit from longer time series observations of multiple active lava lobes to further explore the statistical significance of the relationship between areal spreading and inflation.

Comparisons between model simulations and observations

Given the measured volume of Lobe A and typical parcel volume of 0.09 m^3, Lobe A would include ~117 parcels. The simulation of a lobe composed of 117 parcels begins with a 1×7 cell linear source region trending east–west (depicted as the gray-shaded region in Fig. 11a crossing through the midpoint of the array). This source region, with one parcel in each of the seven cells, is approximately equivalent to the initial length of Lobe A (i.e., ~4.69 m; see Fig. 4a). The model also includes two parallel barriers located at ±3 cells along the north–south axis. The barriers are considered transitional zones in which the advancing lava enters, but becomes blocked, thereby reflecting the lava parcel back toward the interior of the flow. The distance between these barriers is 4.69 m (including the barrier cells as well), which corresponds to the topographically bounded maximum width of Lobe A. The probabilities of sequentially adding 0, 1, or 2 extra parcels from an existing flow margin are $P(0)=P(1)=0.25$ and $P(2)=0.5$.

One cannot expect any specific realization of the stochastic model to exactly reproduce the morphology of an observed lava lobe, but characteristics of the simulated lobes are broadly
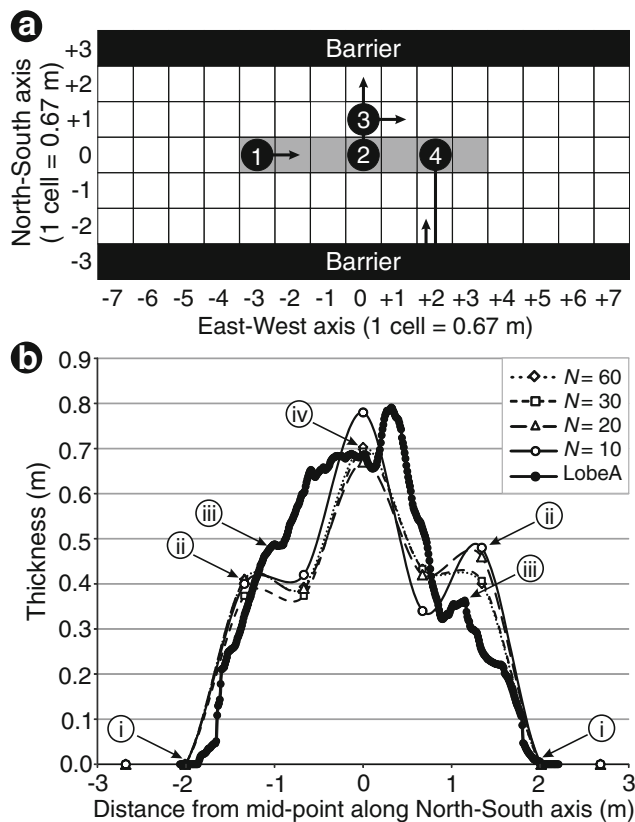
Fig. 11 **a** A schematic example showing how the stochastic model works. A linear source region (shown in *gray*) passes through the mid-point of the array and trends east–west. Two parallel barriers are shown ±3 cells from the linear source along the north–south axis. In the simulation, a cell is first chosen at random from within the confines of the flow (initially corresponding to the extent of the linear source region), and then, a random cardinal direction is chosen. A lava parcel is then transferred to the specified cell (marked with a *filled black circle*, e.g., "1") and to adjacent cell (identified by the *associated arrow*). If the parcel would be allocated beyond the confines of the flow, there is a 0.25, 0.25, and 0.50 probability that 0, 1, or 2 extra parcels, respectively, will be allocated to sequential cells in the same direction (e.g., "2" shows 1 extra, 2 total, cells being added). As the areal extent of the flow increases, new parcel transfer locations become available (e.g., "3"). If a cell allocation would result in a parcel being extended beyond the barrier, then the parcel is reflected back towards the cell interior (e.g., "4"). Each parcel allocated to a given cell increases its thickness by 0.2 m. This process is repeated until all lava parcels are allocated, which in the case of Lobe A includes a total of 117 parcels. **b** Simulated north–south profiles for Lobe A, averaged over 10, 20, 30, and 60 realizations of the model. The results show that despite the stochastic nature of the model, the average simulations converge to a stable equilibrium shape over a few tens of realizations though there remains persistent topographic variations. Also shown is the flow-perpendicular cross-section though Lobe A (Fig. 4b) with the underlying topographic trend removed. *i* The maximum width-simulated lobes and Lobe A are determined by the influences of topographic barriers. *ii* Reflecting of lava parcels by the barriers produces an excess thickening in the adjacent interior cells. *iii* High-standing topography and stagnated peripheral toes help to confine the interior of the lobe and promote inflation. *iv* The thickest portion of the simulated lobe is located along the medial axis and is generally consistent with the thickness of Lobe A along the flow axis

consistent with the morphology of Lobe A. Figure 11b shows examples of topographic profiles taken perpendicular to the

flow direction through the simulated lobes averaged over 10, 20, 30, and 60 realizations. These examples demonstrate that there are stochastic variations between simulations, but also persistent morphological characteristics. For example, the simulated lobes are thickest in the middle (i.e., along the axis of the linear source region) with maximum heights that are consistent with those observed for Lobe A. The models also exhibit the effects of lava confinement along lobe margins due to lava parcels being reflected back toward the interior of the flow. Plan views of the simulated lobes (e.g., Fig. 9) also show irregular margins and thickness variations that are typical of inflated pāhoehoe lobes.

Discussion

Relationships between pāhoehoe breakouts and inflation

Pāhoehoe breakouts will be emplaced with some initial thickness and then grow through a process of inflation. This inflation process includes two dominant components: thickening of the molten core and thickening of the crust (Hon et al. 1994), with the crust consisting of both a brittle outer layer and underlying viscoelastic layer. After an initial chilled margin forms around a new toe, it will retain incoming lava and inflate as its molten core thickens to equalize the pressure with other connected portions of the fluid lava pathway. During the early stages of emplacement, the rate of core thickening will greatly exceed the rate of crustal thickening (Hon et al. 1994), but as the fluid interior achieves its equilibrium thickness, inflation will be increasingly dominated by the process of crustal growth (Cashman and Kauahikaua 1997).

Two conditions must be met for the upper crust to continue to accrete a new material and contribute to inflation. First, there must be a continuous influx of new lava through the molten core and, second, there must be physical coupling of the molten core to the upper crust (Kauahikaua et al. 1998). If the flow of lava through the core stagnates, then the lava will cool in situ and will not increase the flow's total thickness. Additionally, if the molten core partially drains and decouples from the upper crust, then the new material will not be added to the base of the surface layer and the crust may even subside and "deflate" (Kauahikaua et al. 1998). Cooling histories inferred from the thicknesses of the upper brittle and viscoelastic layers (Hon et al. 1994) therefore provide an estimate of the time that a lava pathway flowed at full capacity, but not necessarily the total duration of emplacement if the core of the flow and the upper crust were decoupled. In some cases, the molten core of a flow can also undergo cycles of pressurization related to changes in the local discharge rate (Orr 2011). This can lead to variations in molten core pressure that induce cycles of surface disruption and subsidence, thereby producing a range of surface textures, including slabbly pāhoehoe,

rubbly pāhoehoe, and shatter rings (Keszthelyi et al. 2000, 2006; Guilbaud et al. 2005; Orr 2011).

Initial cooling can strengthen the margins of a lava flow (Castruccio et al. 2013), but the process is complicated by the development of numerous cooling fractures. These fractures will mechanically weaken the outer brittle crust and make the underlying viscoelastic layer more important in terms of governing the overall confining strength of the flow. The frequency of breakouts will therefore depend on the balance between the combined strength of the brittle and viscoelastic layers relative to the pressure within the molten core (Hoblitt et al. 2012). If the internal pressure exceeds the confining strength of the flow's outer layers, then the periphery of the flow will rupture and generate new breakouts that promote increased areal growth. In contrast, if the exterior of the flow does not rupture, it will pressurize and inflate through gradual deformation of the viscoelastic layer and opening of fractures in the overlying brittle crust.

In this study, peripheral lobes along the margins of the PKK flow on the flanks of Kīleaua Volcano exhibited a generally constant local discharge rate (0.0061 ± 0.0019 m²/s). However, approximately every 4 min, there was a significant increase in the areal spreading rate. The observed periodicity in areal coverage may relate to the changing balance between the confining strength of the lava as it cools and strengthens and the internal pressure within the core of the flow. This balance would give rise to an increased frequency of new breakouts when the core pressure exceeds the confining strength of the exterior. Enhanced areal spreading rates would then persist until the core pressure decreases below a critical threshold required to continuously rupture the active flow margin. As the rate of areal spreading deceases, continued influx of lava into the lobe would begin to re-pressurize its fluid core and perpetuate a new cycle. This process, operating on the scale of an individual lobe, is similar to what Hoblitt et al. (2012) have observed on the scale of an entire pāhoehoe flow, which demonstrates the self-similarity of the inflation mechanism over a range of scales.

Static and dynamic pressure considerations

During early stages of pāhoehoe emplacement, the inflation process will be dominated by molten core thickening as the liquid interior of the flow moves toward an equilibrium thickness. However, there are multiple factors that can contribute to this equilibrium. Calculations generally assume a Bingham liquid rheology, with lava descending a slope as an unconfined laminar flow under the influence of gravity (Hulme 1974; Dragoni et al. 1986; Castruccio et al. 2013). Within this scenario, the critical depth h_s required to induce down-slope flow will be

$$h_s = \sigma_0 / \rho g sin(\beta) \tag{2}$$

where σ_0 is the flow's yield stress, ρ is the flow's density, g is the gravitational acceleration, and β is the underlying slope (see Eq. (14) in Hulme 1974). However, calculations of a lava flow's equilibrium thickness will be complicated by cooling-induced changes in rheology and other factors that influence its internal pressure. Several studies (e.g., Rossi and Gudmundsson 1996; Anderson et al. 1999, 2012) have considered the "magmastatic" pressure (herein referred to as "hydrostatic" pressure) generated by fluid elevation changes along hydrostatically connected pathways, as well as the pressure required to drive lava through pipe-like pathways and lift the crust. These models generally assume that the pathways (i.e., lava tubes) are cylindrical pipes with constant cross-sectional area, but the geometry of lava pathways can vary widely within a pāhoehoe flow (e.g., Guest et al. 1984; Kauahikaua et al. 1998; Self et al. 1998; Calvari and Pinkerton 1999). This raises the possibility that changes in pathway geometry can introduce additional changes in lava core pressure due to dynamic processes.

These dynamic effects may be understood within the context of Bernoulli's principle, which describes the inverse relationship between fluid flow velocity and fluid pressure within incompressible laminar flows through a pipe (Resnick and Halliday 1977; Batchelor 1980). Within a lava flow, changes in fluid core pressure could affect inflation rates by changing the magnitude of the stresses applied to the overlying crust. This may lead to increased inflation rates where the flow velocity decreases and the core pressure increases. Conversely, inflation rates would be lower where the flow velocity increases and the core pressure decreases. For otherwise equivalent lava flows through a pipe-like pathway, the most important controls on fluid velocity will be the pipe's cross-sectional area and underlying slope. In general, lava velocities will be relatively low where the flow pathway is broad and its cross-sectional area is large and/or where it descends a shallow slope or encounters a reverse-facing slope. Alternatively, flow velocities will be higher when lava enters a narrow topographic constriction and/or descends a steeper slope. These scenarios are broadly consistent with the observed relationship between the initial topography and final morphology for Lobe B. In this case, maximum inflation was observed where the flow was the broadest and above shallow to reverse-facing slopes, whereas the least inflation was observed where the flow passed through narrow constrictions and descended steep slopes (Figs. 6 and 7). These observations support the viability of a conservation of energy approach to modeling the spatial variability of inflation and its relationship to emplacement processes. Early stage inflation processes related to core pressurization and thickening may also help to establish preferred pathways through the thickest parts of the flow, which would continue to preferentially inflate through crustal accretion if the pathways remain full. Continued crustal accretion and uplift must also be coupled with overpressurization of the molten core, which Cashman and Kauahikaua (1997) inferred

from their observations of pāhoehoe crustal vesicularity profiles that exhibit decreased vesicle number density with depth. These examples highlight the importance of considering both fluid static and dynamic components in models of pāhoehoe inflation.

Conclusions

The confining strength of a lava lobe depends strongly on the age distribution of its surfaces, with the youngest surfaces (i.e., sites of the most recent breakouts) being the weakest. Therefore, when new breakouts occur, growth tends to concentrate at these localities. Otherwise, the next most likely location for a breakout to occur is from an older fractured surface overlying a still molten core. This process is treated with a stochastic model by introducing correlation with a probability distribution describing the preferential growth of the flow in the direction of new breakouts through sequential emplacement of lava parcels (i.e., toes) from that locality. Including correlated growth into the model also recreates observed periods of enhanced areal spreading and lobe morphologies.

Time series data for Lobe A shows that periods of enhanced areal spreading roughly alternate with periods of increased excess volume change. For an approximately constant local discharge rate, this suggests that the volume of lava not utilized during the process of areal spreading can contribute to thickening through inflation. Trade-offs between areal spreading and inflation should be detectable in thermal infrared (e.g., FLIR) imagery, provided that a single lobe is isolated in the field of view. For instance, when the flow enters a period of above average areal spreading, newly exposed lava surfaces will radiate more thermal energy and will contribute to an increased frequency distribution of high temperature pixels within the field of view. As the flow shifts toward an inflation-dominated mode, older lava surfaces will cool dominantly by conduction rather than radiation (Hon et al. 1994), and this would shift the frequency distribution of temperatures toward lower values. Temperature distributions in FLIR data may therefore be used to identify the patterns of pāhoehoe flow emplacement, such as periodicities in areal spreading rate and the trade-off with inflation. Statistical models of flow emplacement may be improved by coupling them with a cooling model to estimate the temperature distribution of the lava based on its emplacement age.

New toes are highly sensitive to subtle topographic irregularities, and for low-discharge rate, flows may be deflected or stopped by obstacles measuring only a few centimeters in height. This process was observed during the emplacement of Lobe B and demonstrates that the final morphology of a lobe may inherit boundaries influenced by variations in the initial toe-scale topography that are orders of magnitude smaller than the flow's final thickness. Even though toes may be locally deflected or impeded by toe-scale topography, inflating pāhoehoe lobes may overcome local barriers through a combination of stochastic breakouts in down-flow and cross-flow directions that allow them to find and follow the maximum regional slope. These behaviors are described in the model by considering the sequential emplacement of new lava parcels (i.e., toes) from existing flow margins, with boundaries that reflect parcels back towards the interior of the flow.

Combining measurements of initial topography with time series observations of active pāhoehoe lobes provides new insights into the growth of pāhoehoe flows. These observational constraints also help to improve statistical models of lava emplacement processes and better understand the relationship between areal expansion and inflation. This information is important for understanding how subtle topographic influences can be inherited by inflated lobes to develop preferred lava pathways that influence the overall development of pāhoehoe lava flows on Earth and other planetary surfaces.

References

Anderson SW, Stofan ER, Smrekar SE, Guest JE, Wood B (1999) Pulsed inflation of pahoehoe lava flows: implications for flood basalt emplacement. Earth Planet Sci Lett 168:7–18

Anderson SW, Smrekar SE, Stofan ER (2012) Tumulus development on lava flows: insights from observations of active tumuli and analysis of formation models. Bull Volcanol 74:931–946. doi:10.1007/s00445-012-0576-2

Baloga S (1987) Lava flows as kinematic waves. J Geophys Res 92(B9):9271–9279

Baloga S, Glaze LS (2003) Pahoehoe transport as a correlated random walk. J Geophys Res 108:2031. doi:10.1029/2001JB001739

Baloga S, Glaze LS (2008) Self-replication model for long channelized lava flows on the Mars plains. J Geophys Res 113, E05003. doi:10.1029/2007JE002954

Baloga S, Pieri DC (1986) Time-dependent profiles of lava flows. J Geophys Res 91:9543–9552

Batchelor GK (1980) An introduction to fluid dynamics. Cambridge Univ Press, New York, 615 p

Bruno BC, Taylor GJ, Rowland SW, Baloga SM (1994) Quantifying the effect of rheology of lava-flow margins using fractal geometry. Bull Volcanol 56:193–206

Byrnes JM, Crown DA (2001) Relationships between pahoehoe surface units, topography, and lava tubes at Mauna Ulu, Kilauea Volcano, Hawaii. J Geophys Res 106(B2):2139–2151

Calvari S, Pinkerton H (1999) Lava tube morphology on Etna and evidence for lava flow emplacement mechanisms. J Volcanol Geotherm Res 90:263–280

Cashman KV, Kauahikaua JP (1997) Reevaluation of vesicle distributions in basaltic lava flows. Geology 25:419–422. doi:10.1130/0091-7613

Castruccio A, Rust AC, Sparks RJS (2013) Evolution of crust- and core-dominated lava flows using scaling analysis. Bull Volcanol 75:681. doi:10.1007/s004455-012-0681-2

Crisp JA, Baloga SM (1990) A model for lava flows with two thermal components. J Geophys Res 95:1255–1270

Crown DA, Baloga SM (1999) Pahoehoe toe dimensions morphology, and branching relationships at Mauna Ulu, Kilauea Volcano, Hawai'i. Bull Volcanol 61:288–305

Danes ZF (1972) Dynamics of lava flows. J Geophys Res 77:1430–1432

Day T, Muller JP (1989) Digital elevation model production by stereo-matching SPOT image-pairs: a comparison of algorithms. Image Vision Comput 7:95–101

Doane DP (1976) Aesthetic frequency classifications. Am Stat 30:181–1905

Dragoni M, Bonafede M, Boschi E (1986) Downslope models of a Bingham liquid: implications for lava flow. J Volcanol Geotherm Res 30:305–325

Glaze LS, Baloga SM (2013) Simulation of inflated pahoehoe lava flows. J Volcanol Geotherm Res 255:108–123. doi:10.1016/j.jvolgeores.2013.01.018

Gruen AW (1985) Adaptive least squares correlation: a powerful image matching technique. S Afr J Photogramm Remote Sens Cartogr 14:175–187

Guest JE, Wood C, Greeley R (1984) Lava tubes, terraces and megatumuli on the 1614–24 pahoehoe lava flow field, Mount Etna, Sicily. Bull Volcanol 47(3):635–648

Guilbaud M-N, Self S, Thordarson T, Blake, S (2005) Morphology, surface structures and emplacement of lavas produced by Laki, AD 1783–1874. In: Manga M, Ventura G (eds) Kinematics and dynamics of lava flows (Special Papers No. 396). Geological Society of America, pp 81–102

Hamilton CW, Thordarson T, Fagents SA (2010) Explosive lava–water interactions I: architecture and emplacement chronology of volcanic rootless cone groups in the 1783–1784 Laki lava flow, Iceland. Bull Volcanol 72(4):449–467. doi:10.1007/s00445-009-0330-6

Harris AJL (2013) Lava flows. In: Fagents SA, Gregg TKP, Lopes RMC (eds) Modeling volcanic processes: the physics and mathematics of volcanism. Cambridge University Press, New York, pp 85–106

Harris AJL, Rowland SK (2001) FLOWGO: a kinematic thermo-rheological model for lava flowing in a channel. Bull Volcanol 63:20–44

Harris AJL, Rowland SK (2009) Effusion rate controls on lava flow length and the role of heat loss: a review. In: Thordarson T, Self S, Larsen G, Rowland SK, Hoskuldsson A (eds) Studies in volcanology: the legacy of George Walker (Special Publication of IAVCEI No. 2). Geological Society, London, pp 33–51

Harris AL, Dehn J, James MR, Hamilton C, Herd R, Lodato L, Steffke A (2007a) Pahoehoe flow cooling, discharge, and coverage rates from thermal image chronometry. Geophys Res Lett 34, L19303. doi:10.1029/2007GL030791

Harris AJL, Dehn J, Calvari S (2007b) Lava effusion rate definition and measurement: a review. Bull Volcanol 70:1–22

Heliker C, Mattox TN (2003) The first two decades of the Pu'u 'Ō'ō–Kūpaianaha eruption: chronology and selected bibliography. In: Heliker C, Swanson DA, Takahashi TJ (eds) The Pu'u 'Ō'ō–Kūpaianaha eruption of Kīlauea volcano, Hawai'i the first 20 years. USGS Professional Paper 1676, pp 1–28

Hoblitt RP, Orr TR, Heliker C, Denlinger RP, Hon K, Cervelli PF (2012) Inflation rates, rifts, and bands in a pāhoehoe sheet flow. Geosphere 8(5):179–195. doi:10.1130/GES00656.1

Hon K, Kauahikaua J, Denlinger R, MacKay R (1994) Emplacement and inflation of pahehoe sheet flows: observations and measurements of active lava flows on Kilauea Volcano, Hawaii. Geol Soc Am Bull 106:351–370

Hulme G (1974) The interpretation of lava flow morphology. Geophys J R astr Soc 39:361–383

Kauahikaua J, Cashman KV, Mattox TN, Heliker CC, Hon LA, Mangan MT, Thornber CR (1998) Observations on basaltic lava streams in tubes from Kilauea Volcano, island of Hawai'i. J Geophys Res 103(B11):27,303–27,323

Keszthelyi L, Denlinger R (1996) The initial cooling of pahoehoe flow lobes. Bull Volcanol 58:5–18

Keszthelyi L, Self S, Thordarson T (1999) Application of recent studies on the emplacement of basaltic lava flows to the Deccan Traps. Mem Geolog Soc India 43:485–520

Keszthelyi L, McEwen AS, Thordarson T (2000) Terrestrial analogs and thermal models for Martian flood lavas. J Geophys Res 105(E6):15,027–15,049

Keszthelyi L, Self S, Thordarson T (2006) Flood lavas on Earth, Io and Mars. J Geol Soc 163(2):253–264

Kilburn CRJ (1996) Patterns and predictability in the emplacement of subaerial lava flows and flow fields. In: Scarpa R, Tilling RI (eds) Monitoring and mitigation of volcanic hazards. Springer, New York, pp 491–537

Koeppen WC, Patrick M, Orr T, Sutton AJ, Dow D, Wright R (2013) Constraints on the portioning of Kīlauea's lavas between surface and tube flows, estimated from infrared satellite data, sulfur dioxide emission rates, and field observations. Bull Volcanol 75:716. doi:10.1007/s00445-013-0716-3

Orr TR (2011) Lava tube shatter rings and their correlation with lava flux increases at Kīlauea Volcano, Hawai'i. Bull Volcanol 73:355–346. doi:10.1007/s00445-010-0414-3

Otto GP, Chau TKW (1989) Region-growing algorithm for matching of terrain images. Image Vision Comput 7:83–94

Peitersen MN, Crown DA (2000) Correlations between topography and intraflow width behavior in Martian and terrestrial lava flows. J Geophys Res 105(E2):4123–4123

Poland MP, Miklius A, Jeff Sutton A, Thornber CR (2012) A mantle-driven surge in magma supply to Kilauea Volcano during 2003–2007. Nat Geosci 5(4):295–300

Resnick R, Halliday D (1977) Physics: part one, 3rd ed. Wiley, New York, 608 p

Robson S, James MR (2007) Photogrammetric image sequence processing to determine change in active lava flows. Proc Remote Sensing and Photogrammetry Society Ann Conf, 2007 (RSPSoc 2007), 11–14th September, Newcastle upon Tyne, U.K.

Rossi MJ, Gudmundsson A (1996) The morphology and formation of flow-lobe tumuli and Icelandic shield volcanoes. J Volcanol Geotherm Res 72:291–308

Rowland SK, Harris AJL, Garbeil H (2004) Effects of Martian conditions on numerically modeled, cooling-limited channelized lava flows. J Geophys Res 109(E10010). doi:10.1029/2004JE002288

Self S, Thordarson T, Keszthelyi L, Walker GPL, Hon K, Murphy MT, Long P, Finnemore D (1996) A new model for the emplacement of Columbia River basalts as large, inflated pahoehoe lava flow fields. Geophys Res Lett 23:2689–2692

Self S, Thordarson T, Keszthelyi L (1997) Emplacement of continental flood basalt lava flows. Am Geophys Union Monograph 100:381–410

Self S, Keszthelyi L, Thordarson T (1998) The importance of pāhoehoe. Ann Rev Earth Planet Sci 26(1):81–110

Sheskin DJ (2011) Handbook of parametric and nonparametric statistical procedures, 5th edn. Chapman and Hall/CRC, New York, p 1926

Smith WHF, Wessel P (1990) Gridding with continuous curvature splines in tension. Geophysics 55(3):293–305

Sturges H (1926) The choice of a class-interval. J Am Stat Assoc 21:65–66

Thordarson T, Self S (1998) The Roza Member, Columbia River Basalt Group: a gigantic pahoehoe lava flow field formed by endogenous processes? J Geophys Res 103(B11):27411–27445

Walker GPL (1991) Structure, and origin by injection of lava under surface crust, of tumuli, 'lava rises', 'lava-rise pits', and 'lava-inflation clefts' in Hawaii. Bull Volcanol 53:546–558

Walker GPL (2009) The endogenous growth of pahoehoe lava lobes and morphology of lava-rise edges. In: Thordarson T, Self S, Larsen G, Rowland SK, Hoskuldsson A (eds) Studies in volcanology—the legacy of George Walker (Special Publications of IAVCEI No. 2). The Geol Soc: pp 17–32

Wilmoth RA, Walker GPL (1993) P-type and S-type pahoehoe: a study of vesicle distribution and patterns in Hawaiian lava flows. J Volcanol Geotherm Res 55:129–142